GEOPHYSICS, VOL. 57, NO. 10 (OCTOBER 1992); P. 1359–1372, 13 FIGS., 1 TABLE.

Characteristics and processing of seismic data collected on thick, floating ice: Results from the Ross Ice Shelf, Antarctica

Bruce C. Beaudoin*, Uri S. ten Brink‡, and Tim A. Stern**

ABSTRACT

Coincident reflection and refraction data, collected in the austral summer of 1988/89 by Stanford University and the Geophysical Division of the Department of Scientific and Industrial Research, New Zealand, imaged the crust beneath the Ross Ice Shelf, Antarctica. The Ross Ice Shelf is a unique acquisition environment for seismic reflection profiling because of its thick, floating ice cover. The ice shelf velocity structure is multilayered with a high velocity-gradient firn layer constituting the upper 50 to 100 m. This near surface firn layer influences the data character by amplifying and frequency modulating the incoming wavefield. In addition, the ice-water column introduces pervasive, high energy seafloor, intra-ice, and intra-water multiples that have moveout velocities similar to the expected subseafloor primary velocities. Successful removal of these high energy multiples relies on predictive deconvolution, inverse velocity stack filtering, and frequency filtering. Removal of the multiples reveals a faulted, sedimentary wedge which is truncated at or near the seafloor. Beneath this wedge the reflection character is diffractive to a two-way traveltime of ~7.2 s. At this time, a prominent reflection is evident on the southeast end of the reflection profile. This reflection is interpreted as Moho indicating that the crust is ~21-km thick beneath the profile. These results provide seismic evidence that the extensional features observed in the Ross Sea region of the Ross Embayment extend beneath the Ross Ice Shelf.

INTRODUCTION

Multichannel seismic reflection data collected on floating ice are typically confined to thin (≤10 m) sea ice. Thin sea ice constitutes an approximately constant velocity layer and sound sources can easily be suspended beneath the ice (Kim et al., 1986) or conventional vibrators can be used (Mertz et al., 1981). Data from these environments include flexural ice waves [see Press and Ewing, (1951)] and near-surface multiples. Flexural ice waves can be successfully suppressed during acquisition (Proubasta, 1985; Rendleman and Levin, 1990) and with specialized filtering techniques (Beresford-Smith and Rango, 1988). Unwanted multiple phases are often successfully removed with predictive deconvolution and velocity filters. Unlike regions of sea ice, the Ross Ice Shelf, Antarctica is a unique environment of thick ice (200 to 850 m) with a compressional-wave velocity of 3800 m/s overlying 0 to 900 m of lower-velocity water (1440 m/s). The ice shelf's velocity structure is multilayered with a high velocity-gradient firn layer constituting the upper 50 to 100 m. Firn, as used here, includes the surface snow cover; snow becomes firn after one melt season and firn becomes glacial ice when permeability to liquid water drops to zero. The thickness of the ice shelf requires sound sources to be located either on the surface or within this high velocity-gradient layer. Although the ice shelf is too thick to produce flexural ice waves (Press and Ewing, 1951), the firn and ice lid influence the data character by introducing strong multiples, altering the shape of the wavelet, and altering the frequency content of the data.

During the austral summer of 1988/89, Stanford University and the Geophysics Division of the Department of Scientific and Industrial Research (DSIR), New Zealand, collected a 58-km-long reflection profile and a coincident 31.1-km-long refraction profile (Figure 1). The reflection profile is the

Manuscript received by the Editor September 11, 1991; revised manuscript received March 11, 1992.
*Department of Geophysics, Stanford University, Stanford, CA 94305.
‡formerly Department of Geophysics, Stanford University, Stanford, CA 94305; presently U.S. Geological Survey, Woods Hole, MA 02540.
**formerly Department of Scientific and Industrial Research, Wellington, New Zealand; presently Research School of Earth Sciences, Victoria University of Wellington, Wellington, New Zealand.

longest multichannel seismic profile collected to date in the interior of Antarctica and presented both logistical and processing challenges. The objectives of this experiment were twofold: (1) to study the lithospheric flexure associated with the emplacement of the Cenozoic volcanics of the Ross Archipelago (Figure 1) and (2) to test acquisition techniques and develop a processing scheme for future reflection work in Antarctica. The first experimental objective is discussed in a companion paper (ten Brink et al., in preparation). The second objective is the topic of this paper.

GEOLOGIC SETTING

The Ross Embayment is comprised of the Ross Sea and the Ross Ice Shelf (Figure 1). Bounding the embayment to the south and east are the Transantarctic Mountains and to the west Marie Byrd Land. Much of the geophysical data available on the Ross Embayment has been collected in the Ross Sea due to its relative ease of access. In the Ross Sea, three sedimentary basins have been identified using seismic methods (Davey et al., 1983). Sediments in these basins are in excess of 3-km thick with possibly as much as 12 km of Oligocene or younger strata in the Victoria Land Basin (Cooper and Davey, 1985). Cooper and Davey (1985) and Cooper et al. (1987) suggest that the Victoria Land Basin is an extensional feature based on its seismic and gravity signatures. Jurdy (1978) and more recently Stock and Molnar (1987) have demonstrated the need for extension between East and West Antarctica using plate tectonic circuits. The amount of extension is estimated at 200 to 255 km in the last 50 My (Fitzgerald et al., 1986; Kamp and Fitzgerald, 1987) and at 350 to 400 km since Jurassic (Behrendt and Cooper, 1991). Seismic refraction and wide-angle reflection profiling in the Ross Sea indicate that the crust beneath this region of the Ross Embayment is 17- to 21-km thick (McGinnis et al., 1985; Cooper et al., 1987; Trehu et al., 1989). Based on the above evidence, high heat flow (Blackman et al., 1987) and the chemistry of the alkaline lavas (Kyle and Cole, 1974), most researchers agree the Ross Embayment is underlain by rifted continental crust (e.g., Behrendt and Cooper, 1991).

The extensional features observed in the Ross Sea are postulated to extend beneath the Ross Ice Shelf based on radio echo sounding, gravity, magnetic, and seismic surveys (Jankowski and Drewry, 1981; Robertson et al., 1982; Bentley, 1983; Robinson and Splettstoesser, 1984; Behrendt and Cooper, 1991). To date, the majority of the seismic refraction and reflection work on the Ross Ice Shelf has focused on

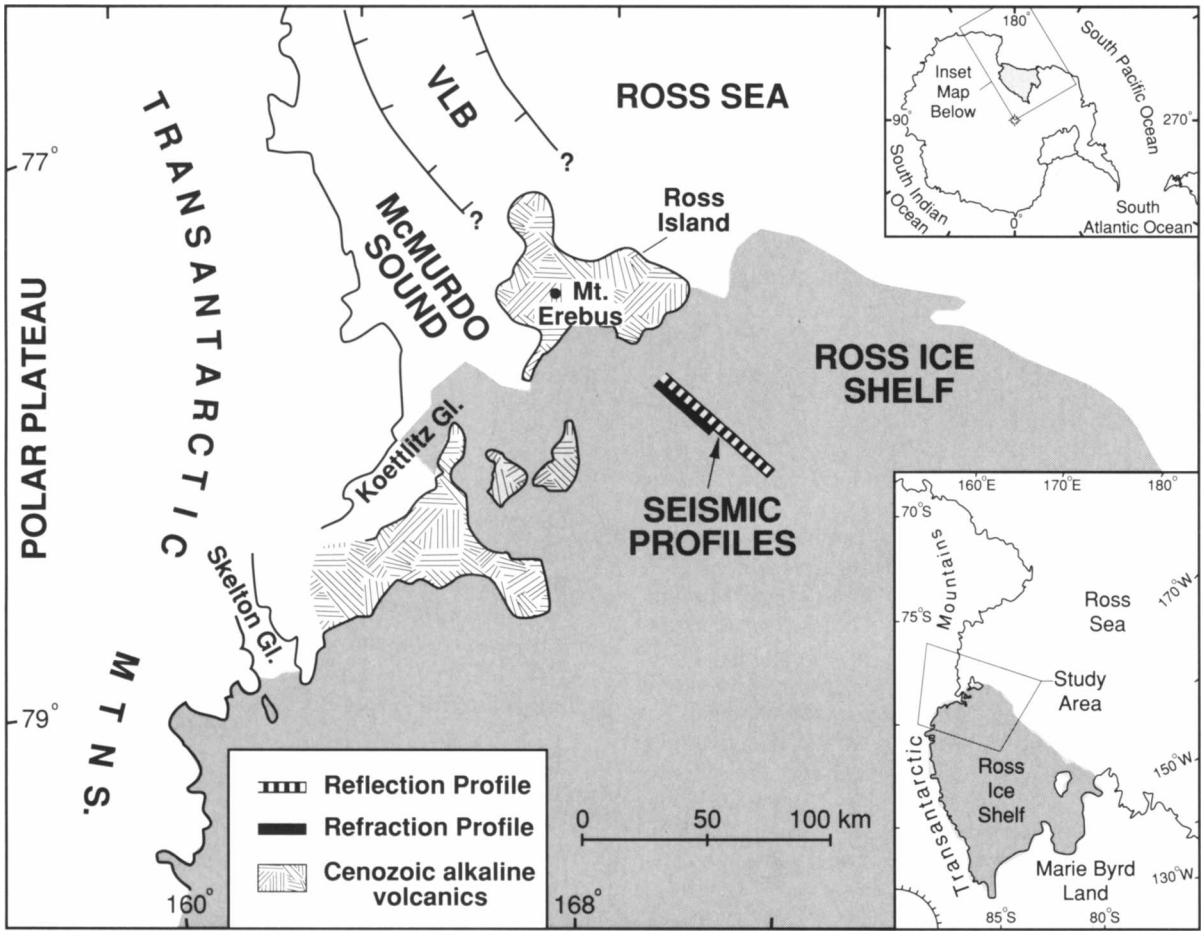

FIG. 1. Map showing the location of the seismic reflection and refraction profiles. The profiles are aligned approximately perpendicular to the Cenozoic alkaline volcanics of the Ross Archipelago. Active rifting is occurring in the Victoria Land Basin (VLB) (Cooper and Davey, 1985).

the ice shelf's morphology and near-seafloor sediments (Thiel and Ostenso, 1961; Crary et al., 1962; Bentley and Jezek, 1981; Robertson et al., 1982; Bentley, 1984). Two short, 5-km-long, multichannel seismic reflection profiles on the Ross Ice Shelf east and southeast of Ross Island were collected in 1985 by DSIR New Zealand (Stern et al., 1991). These data reveal a well stratified sedimentary section of approximately 1-km thickness and a clear unconformity at approximately 200 ms two-way traveltime below the seafloor. The data discussed herein, extend the southernmost of these two profiles.

DATA COLLECTION

The northwest-southeast trending coincident reflection and refraction profiles are located on the Ross Ice Shelf at a point approximately 60 km southeast from the summit of Mt. Erebus (Figure 1). The reflection and refraction profiles extend for 58 km and 31.1 km, respectively. The Department of Survey and Land Information, New Zealand, surveyed the profile location prior to the arrival of the seismic crew. Once the line was surveyed, the seismic and drilling crew established a moving camp beginning at the north end nearest Ross Island. The reflection data were collected at a rate of 4.8 to 9.6 km per day averaging 7.2 km per day. The total duration of the data collection was three weeks, losing six of those days to weather.

Both lines were recorded with a 24-channel Texas Instruments DFS-V. Both single and six phone geophone strings were tested on the ice shelf. The single phone strings were used because of limited time and crew available for data acquisition. The single phones had an extended foot which afforded better coupling in the near surface snow layer, whereas the six phone strings required digging ~0.5 m beneath the surface to get a firm plant. Additionally, field records exhibited little observable difference between the single and six phone strings. These single, 16 Hz geophones were placed at 100 m intervals along the cable. A total of 7.2 km of cable was deployed and the spread geometry was pulled. Cable lengths of 600 m were picked up and redeployed by hand off the back of sledges pulled by skidoos.

The shot holes were drilled with a pressurized hot water drill by Polar Ice Coring Office (PICO) at a rate of six holes per hour, sufficient to maintain a days worth of shot holes ahead of the seismic crew. Shots ranging in size from 4, 5, and 7.5 kg were tested. No observable difference in the field records was recognized between the 5 and 7.5 kg shots. By using a 5 kg charge size, we were able to extend the profile by ~10 km and add the additional dynamite to the refraction sources. These 5 kg shots, 348 in all, were detonated at 200 m intervals in 17-m-deep holes for the reflection profile, affording six-fold coverage. Once the seismic array reached the center of the profile, 28.5 km, a crew was sent back along the line to detonate the refraction shots into the stationary array. These shots (13 in all) ranged in size from 5 to 55 kg of explosives (Table 1) and were spaced at 2.4 km intervals along the northern end of the profile. For each of these large shots, several 17-m-deep holes were used. Each hole was loaded with 5 kg of explosives and the holes were grouped with a spacing of 1.5 m perpendicular to the profile.

A near offset of 300 m was determined to be optimum considering instrument response, near surface arrivals and the need for good primary-multiple phase separation at far offsets for velocity discrimination. One drawback of not having zero offset information is that the reflection off the base of the ice is lost in the ground roll at offsets of greater than ~100 m. During processing, it became apparent that this reflection was crucial for designing accurate prediction filters. Without this reflection, the ice thickness/traveltime had to be calculated using near offset trace multiples that do not have vertical paths.

DATA CHARACTERISTICS

The ice shelf beneath the profile ranges in thickness from 180 m at the northwest end nearest Ross Island to over 300 m on the southeast end (Stern et al., 1991). This thick cover of ice overlies 500 to 800 m of water (Figure 2a). The strong impedance at the ice-water interface and again at the water seafloor interface produces three types of multiples that inundate these data (Figures 2a and 2b): (1) the intra-ice multiple, a short path multiple with separations of less than 200 ms and (2) and (3) seafloor and intra-water multiples, which are both long period multiples with separations of 700 to 1100 ms. Depending on the ice thickness, the shot gathers have distinct characteristics (Figure 2b). In general, primary phases are completely masked by these high energy multiples.

These strong multiples have several striking characteristics. First, the multiples are mostly band limited to frequencies of $\geq$40 Hz (Figure 3). Considering the high attenuation expected in the near surface firn layer (Lang, 1976; Johnson, 1982) this observation is difficult to explain. Second, these band-limited multiples retain high amplitudes throughout the seismic section (Figure 3). Third, the envelope of a single multiple wavelet is Gaussian.

Experimental design and near surface conditions are likely, at least in part, to be responsible for these data characteristics. The 16 Hz geophones will limit energy at the low end of the frequency spectrum; however, this does not explain the marked high frequency amplification of the multiples when comparing $\leq$40 Hz and $\geq$40 Hz (Figure 3). The near surface firn layer has a high velocity-gradient in the upper 10 m (Figure 2a) (Crary et al., 1962; Kohnen and

Table 1. Shot sizes for the refraction profile.

Shot	Offset range (km)	Shot size (kg)
1	0-2.3	7.5
2	2.4-4.7	15.0
3	4.8-7.1	25.0
4	7.2-9.5	25.0
5	9.6-11.9	25.0
6	12.0-14.3	25.0
7	14.4-16.7	25.0
8	16.8-19.1	30.0
9	19.2-21.5	30.0
10	21.6-23.9	25.0
11	24.0-26.3	25.0
12	26.4-28.7	50.0
13	28.8-31.1	55.0

Bentley, 1973). Compressional-wave velocities in the near surface range from 500 m/s at the surface to over 2000 m/s at 10 m depth. In this region, metamorphism of the firn is largely due to packing (Anderson and Benson, 1963; Kohnen and Bentley, 1973; Robertson and Bentley, 1975). From 10 m to approximately 70 m depth, the velocity gradient gradually diminishes. Compressional-wave velocities at these depths range from approximately 2000 m/s to 3800 m/s, the velocity of solid ice. In this region metamorphism of the firn is governed by recrystallization (Anderson and Benson, 1963; Kohnen and Bentley, 1973; Robertson and Bentley, 1975). Below approximately 70 m, any further densification of the ice is by compaction of existing air pockets and has little effect on the velocity. A pressure/temperature-related velocity inversion of ~0.1 km/s occurs at 80 to 100 m in depth and extends to the base of the ice shelf (Robinson, 1968).

NEAR-SURFACE EFFECT ON THE MULTIPLE AMPLITUDE, MULTIPLE FREQUENCY MODULATION, AND THE DIRECT WAVE

Forward modeling was used to better understand the effect that near-surface conditions have on both the direct wave and the multiples in these data; spatial aliasing and the lack of data between 0 and 300 m offsets prevents the use of inversion techniques to model the near surface. This modeling is limited to the thick ice (≥200 m) portions of the profile where the multiples are well separated in time (Figure 2b). One-dimensional (1-D) reflectivity synthetics (Fuchs and Müller, 1971) were used to forward model the aforementioned data characteristics. Full wavefield, vertical component synthetic seismograms were calculated for offsets ranging from 300 to 5000 m and for frequencies ranging from 1 to 90 Hz. The compressional-wave velocity structure (model 1), from top to bottom, used in the synthetics is as follows (Figure 4): a 70-m-thick, high velocity-gradient firn layer, a 270-m-thick ice layer with a velocity of 3800 m/s, a 570-m-thick water layer with a velocity of 1440 m/s, and a half-space with a velocity of 2700 m/s. Shear-wave velocities were calculated from this compressional-wave velocity model using Poisson's ratios ranging from ~0.2 at the surface to 0.33 (Poisson's ratio for glacial ice) at ≥70 m depth (Kohnen and Bentley, 1973). The source wavelet was a spike and the seismograms were calculated to 8 s with a sampling interval of 4 ms. The synthetics were then windowed to offsets of 300 to 2600 m and 0 to 4 s to match the data of interest. For displays of entire shot gathers, each gather has a t^2 gain, and a shot consistent power balance applied. For this reason, only relative amplitudes between

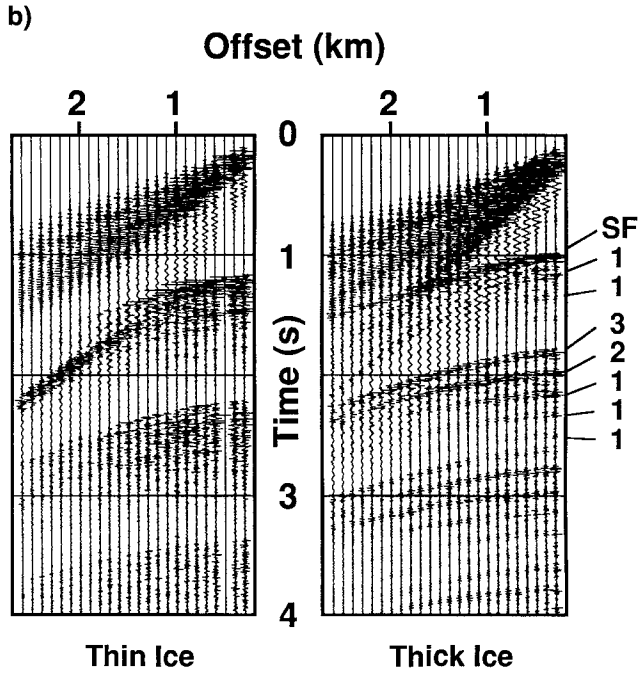

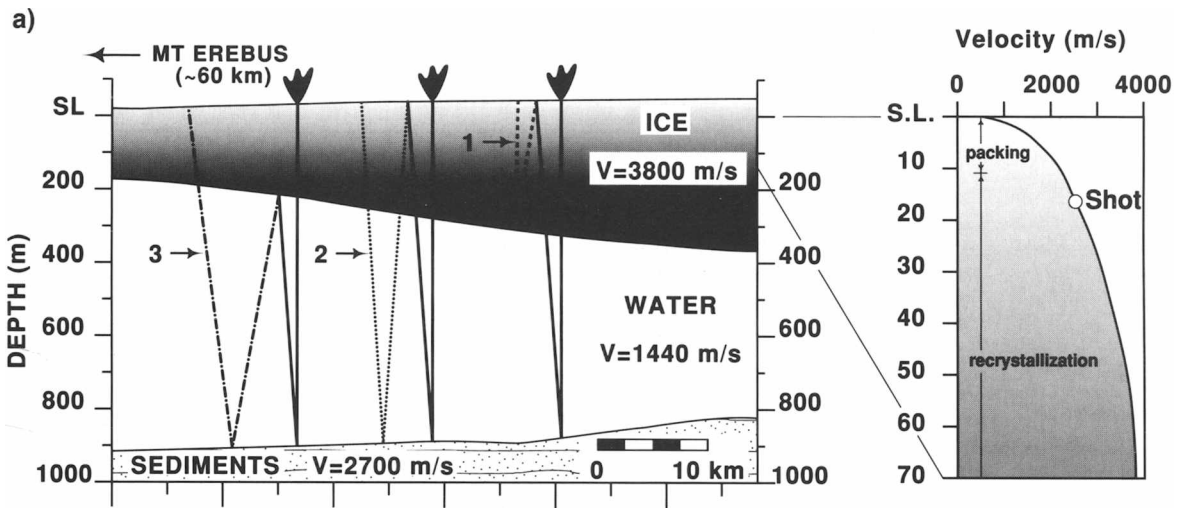

FIG. 2. (a) A cross section of the ice and water thickness along the profile (Stern et al., 1991). The multiple paths shown schematically are: 1 = intra-ice multiple; 2 = seafloor multiple; 3 = intra-water multiple. Path 1 results in short period multiples (≤200 ms). Paths 2 and 3 result in long period multiples (700 to 1100 ms). (b) Characteristic shot gathers for thin (~180 m) and thick (~280 m) ice.

shot gathers can be compared. For displays of individual traces, each trace has t^2 gain applied, and amplitudes can be compared between different models.

Shot depth versus frequency content

The synthetic seismograms predict a strong surface ghost that becomes especially apparent for deeper shots (Figure 4). These strong ghosts interfere both constructively and destructively. Destructive interference manifests in the frequency spectrum as notches (Figure 5).

In comparing the frequency content of a near offset trace from the data with the near offset traces from the models, it is apparent that a strong surface ghost exists in the data (Figure 5). Since the data were generated by 5 kg charges at 17-m depth, a notch in the frequency spectrum is expected to occur in a similar frequency range as the 17-m-depth shot model. However, the data exhibit a higher frequency notch (around 65 Hz as opposed to 45 Hz for the 17-m-depth synthetic) which suggests that the velocity of the firn is higher beneath the array than assumed in the model. The shot depth also governs the partitioning of energy between the direct wave and the surface wave; the deeper the shot, the more energy partitioned into the direct wave and less into the surface wave.

Near-surface layer versus frequency content and amplitude

Although the shot depth modulates the frequency of the source, it does not explain the high amplitudes and the Gaussian envelope observed for both the multiples and the direct wave. Three models, in addition to the previous model (model 1), were used to determine the effect the near-surface velocity structure has on the multiple arrivals (Figure 6). The ice layers in these models are: (model 2) a 70-m-thick, linear velocity-gradient over 270-m-thick, 3800 m/s velocity layer, (model 3) a 70-m-thick, 2770 m/s layer over 270-m-thick 3800 m/s velocity layer, and (model 4) a 340-m-thick, 3540 m/s layer.

All of the models were constructed to maintain a consistent traveltime to the base of the ice. Shot gathers from the data and the various models exemplify the need for the near-surface gradient layer in order to produce the multiple characteristics observed in the data (Figure 6). The multiples in the data exhibit a coda of approximately 100 ms followed by a relatively quiet zone, this pattern is repeated throughout the record section. This characteristic is best matched by model 1. Model 2 begins to exhibit similar multiple characteristics, but does not have the well defined multiples exhibited in model 1. Models 3 and 4 exhibit a much shorter coda

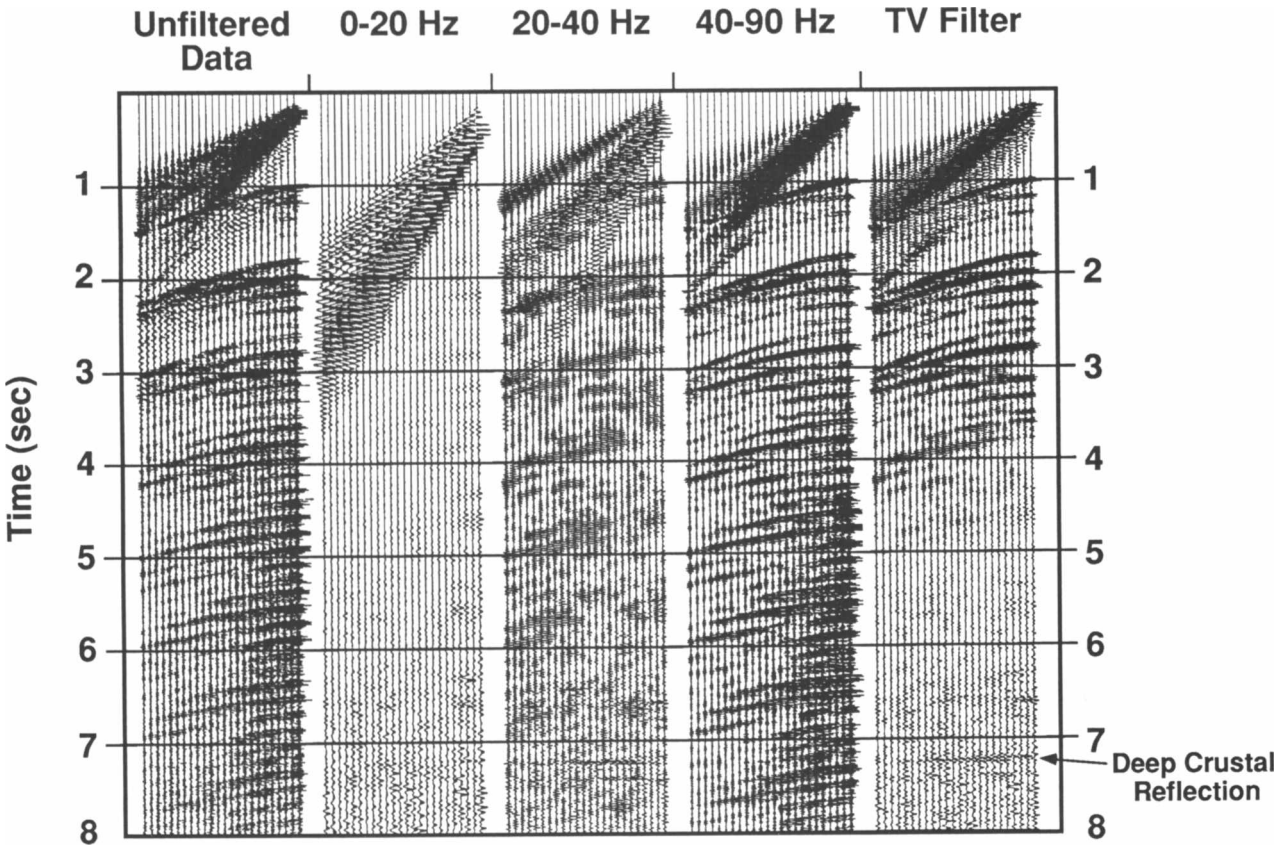

FIG. 3. Frequency panels for a shot from the southeast end of the seismic line. The multiple energy is largely confined to frequencies of ≥40 Hz. The far right panel displays our optimum time-variable (TV) filter.

for each multiple arrival. Model 4 has additional phases that are stronger with increased offset suggesting these might be converted phases.

A closer examination of the near offset traces for the four models shows a complex wavelet for the gradient models (models 1 and 2) and a simple wavelet for the no-gradient models (models 3 and 4) (Figure 7a). The wavelet in the no-gradient models is modified only by the surface ghost and, for model 3 only, by the additional reflection off the bottom of the "firn" layer. Additionally, both gradient models (models 1 and 2) have considerably more energy in the primary and multiple phases. The amplification observed for the primaries and multiples for model 1 is most apparent when frequency filtering these synthetics (Figures 7a and 7b). Only model 1 has considerable amplitudes at the higher frequencies.

We therefore propose that the near-surface, high-gradient layer is amplifying and frequency modulating the incoming wavefield. When a "ray" encounters this layer, the low frequencies have too broad a wavelength to recognize the gradient zone and are reflected as if impinging on a first-order interface (Figure 8). Higher frequencies, on the other hand, sense the gradient zone and become trapped, reverberating within the near-surface layer. For frequencies with associated wavelengths of one quarter the thickness of the gradient zone, amplitudes are optimally enhanced and a Gaussian envelope developed (Figure 8). A similar effect is observed for the ground roll in these data. This phenomena was recognized in earlier seismic work on the Ross Ice Shelf (Robinson, 1968). Robinson documented "pseudo-dispersion" of the direct P-wave because of the waveguide created by the near surface velocity gradient. The spatial sampling of our data, prevented us from duplicating Robinson's approach.

REFRACTION DATA

The refraction data exhibit similar characteristics to the reflection data (Figure 9a): A dispersive direct wave and strong multiples are manifest both in the near offset traces and the shingling of arrivals. The profile is a walk-away gather, consisting of 2.3 km segments associated with indi-

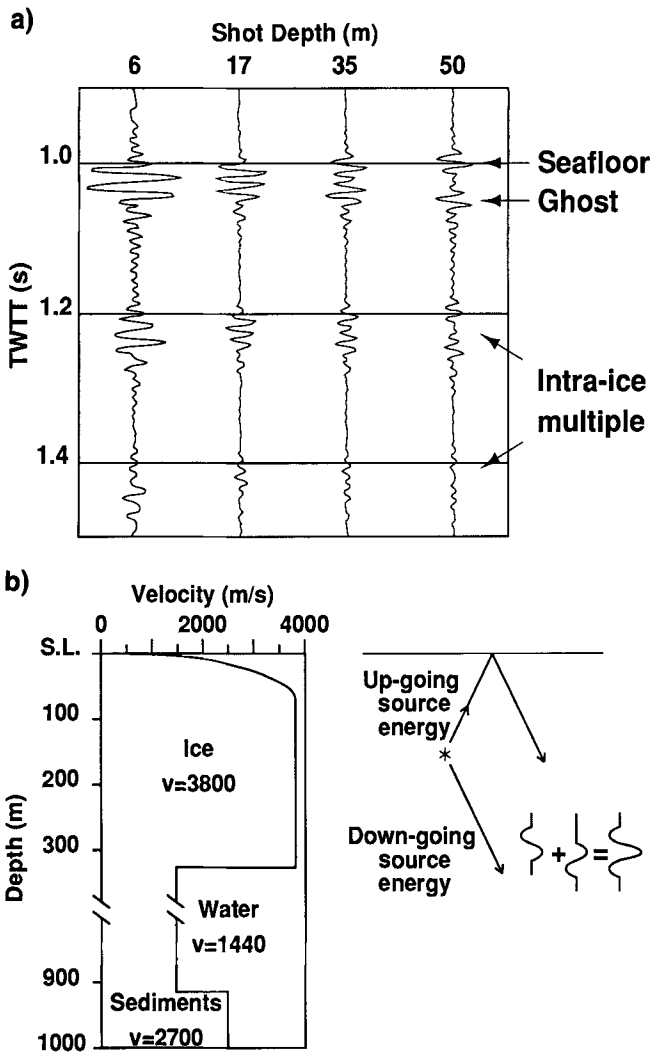

FIG. 4. (a) Unfiltered synthetic seismograms for different shot depths. (b) The compressional-wave velocity function used to generate the synthetic seismograms. A prominent ghost constructively and destructively interferes with the source wavelet.

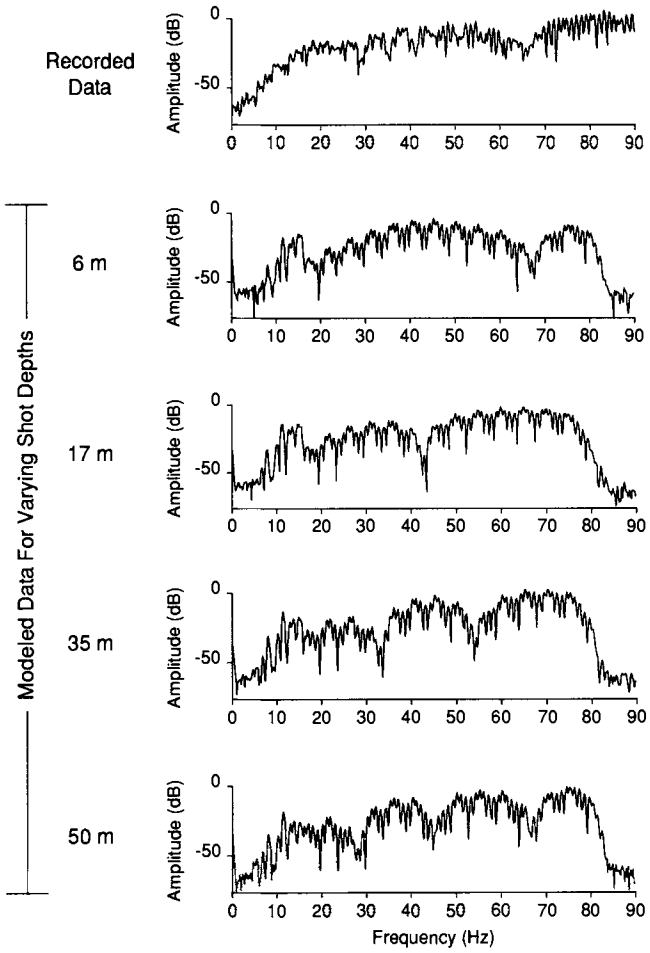

FIG. 5. Frequency spectrum for a near offset data trace and the synthetic traces in Figure 4. Both the data and synthetic traces are unfiltered. The synthetic traces were calculated between 0 to 90 Hz. Note the notches in the frequency spectrum due to destructive interference of the source and ghost.

vidual shots (Table 1). It is evident from these data that shots 10 and 11 (between offsets 20.7 and 25.3 km) were not large enough for good energy propagation, making phase correlation across this region difficult. In addition to the seafloor reflection, three deeper reflections are interpreted, two of which have associated refractions (Figure 9a).

Two refraction models were constructed: (1) a flat layered model to aid in initial reflection stacking, and (2) a dipping layer model based on results from these initial reflection stacks (Figure 9b). Several assumptions were made in modeling these data. First, for both the flat and dipping layer models, the ice thickness and velocity structure were approximated by a constant velocity layer (3554 m/s) derived from the ice thickness profile in Stern et al. (1991) and the velocity profile used in the synthetics above (model 1). Second, for both of these models, the upper 1.5 km of near seafloor layers have velocities based on the reflection profile stacking velocities. Third, for the dipping layer model, the interface geometry is based on several of the more continuous reflections observed on the stacked reflection section. A depth section was then made from the stacked reflection section using the stacking velocities.

The purpose of the refraction modeling was to provide additional velocity information to aid in the reflection processing and interpretation. Since holding the interface geometry fixed is artificial, the traveltimes were fit to within 100 ms; however, our focus was to match the slope of the traveltime curves. Having a fair understanding of the reflector geometry and initial stacking velocities, this approach provided a means to fine tune the reflection stack. It is immediately evident from the refraction profile that the near-sea-floor section is a low-velocity zone (apparent velocities of $\leq$3800 m/s) with respect to the ice layer (Figure 9); there are no refractions associated with layers 1 and 2. This indicates the presence of a sedimentary section beneath the array. As mentioned above, the velocities in these layers are based on stacking velocities. A refraction from layer 3 is evident for a short stretch between 12 to 15 km, and an apparent velocity of ~4600 m/s is calculated for this layer. A crossover at 15 km marks the onset of a basement refraction, layer 4, with an apparent velocity of ~5600 m/s. This phase is identifiable out to 20 km where poor signal-to-noise ratio makes it difficult to correlate. Beyond this point, the basement refraction is inferred to continue to the end of the profile. At offsets of 26 to 30 km there is evidence of a reflection arriving behind the basement refraction, but this phase lacks the lateral extent necessary to provide any velocity information.

REFLECTION PROCESSING

The major challenge faced in the reflection processing was the attenuation of the high energy multiples. Several factors governed our processing approach. First, the band-limited nature of the multiples allowed for frequency filtering to attenuate multiple energy in the later part ($\geq$4 s) of the

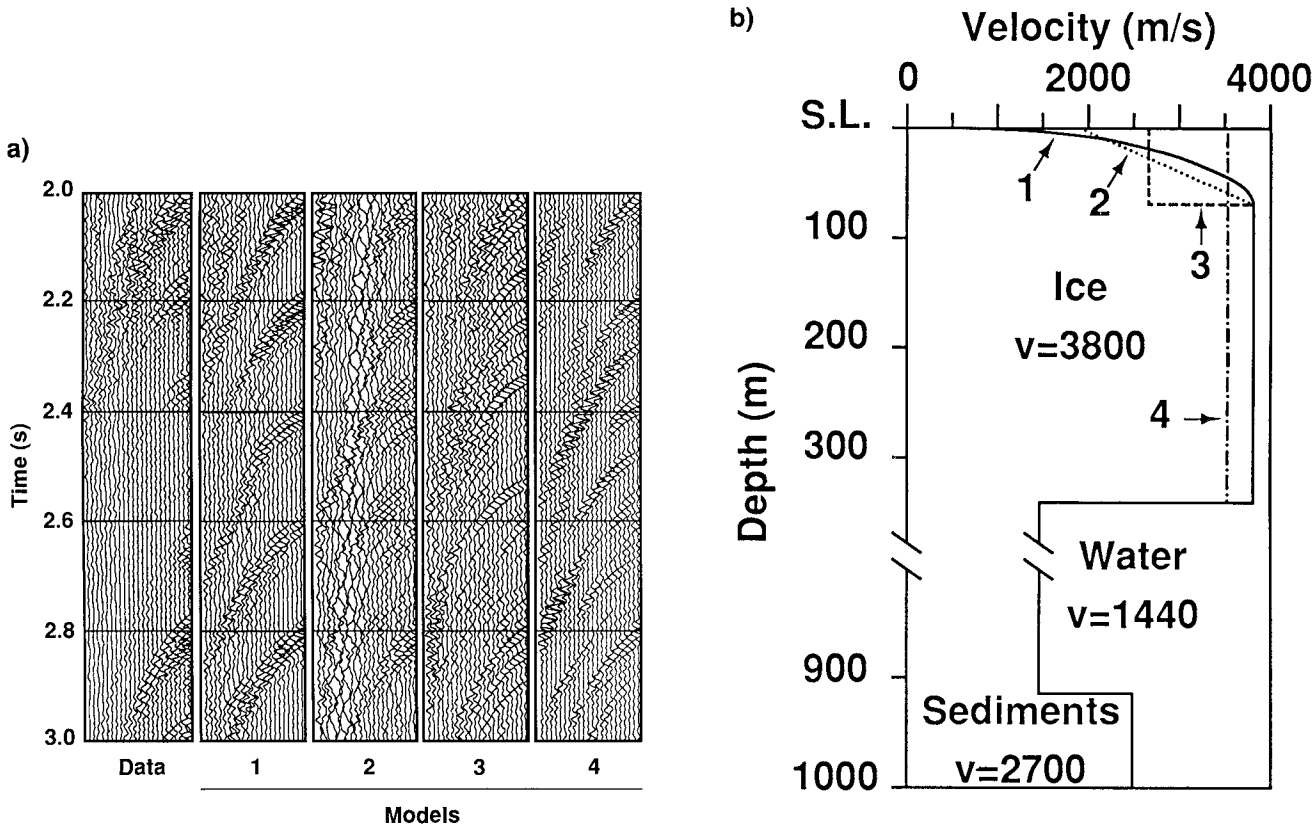

FIG. 6. (a) Unfiltered data and synthetic shot gathers (300 to 2200 m offsets). (b) The compressional-wave velocity models used to generate the synthetics. The decreasing gradient model (model 1) is the only synthetic seismogram that is consistent with the observed data characteristics.

section where primary energy is depleted of the higher frequencies (Figure 3). This low-pass filter was not applied on the upper 3 s of data to retain resolution in the near seafloor region of interest. Second, as previously mentioned, the multiple character varies between regions of thick ice and regions of thin ice (Figure 2). In regions of thick ice, the intra-ice multiples are well separated in time affording the use of predictive attenuation schemes. In regions of thin ice, the intra-ice multiples are poorly separated in time and do not lend themselves to predictive schemes. Although the multiples generated in the thick ice were better suited for removal, their greater amplitudes proved difficult to totally suppress. Third, the intra-ice multiples are problematic since their moveout velocities range from near water velocity to roughly that of solid ice, encompassing the expected range of near the seafloor sediment velocities (Figure 10). This phenomena rules out standard velocity discrimination techniques such as f, k filtering.

The successful removal of multiples from these data was a five step process: (1) gap deconvolution to remove intra-ice multiples in regions of thicker ice, (2) spiking deconvolution along the entire profile, (3) inverse velocity stack filtering to attenuate the longer period intra-water and seafloor multiples, (4) weighted stacking and poststack deconvolution, and (5) frequency filtering to attenuate multiple energy after 4 s in the section.

This paper presents just one scheme for multiple attenuation. Other techniques based on slant stacking (Alam and Austin, 1981) and wave-equation-based prediction (Wiggins, 1988) might work equally as well on these data. However, showing that a modest multiple attenuation scheme can produce significant data improvement provides an important incentive for future research in similar acquisition environments.

Deconvolution

Removal of the near surface intra-ice multiples relies on techniques based on distinguishing the shape of the wavelet and the multiple separately. This requires a multiple time longer than the wavelet. For regions of thin ice (≤200 m; about one fifth of the profile), the intra-ice multiples are not separated well enough in time to obtain significant attenuation using gap deconvolution. However, for the majority of the profile, the intra-ice multiples are well separated in time and the noise level of the data so low that gap deconvolution works extremely well (Figure 11). It was determined that a gap of 85 ms worked best for all shots, coupled with operator lengths varying between 130 to 180 ms.

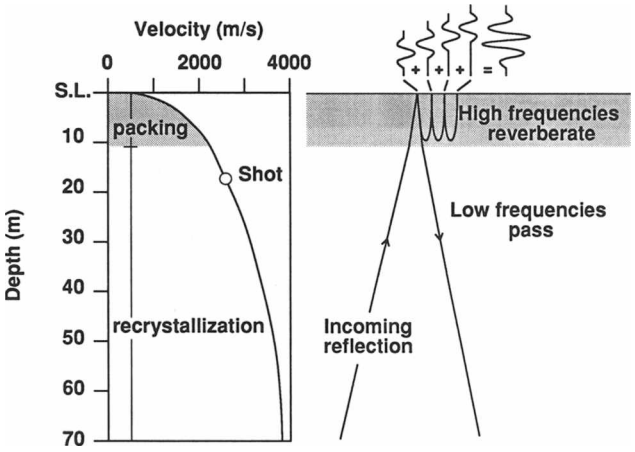

FIG. 8. A cartoon depicting the amplification and frequency modulation of the incoming wavefield.

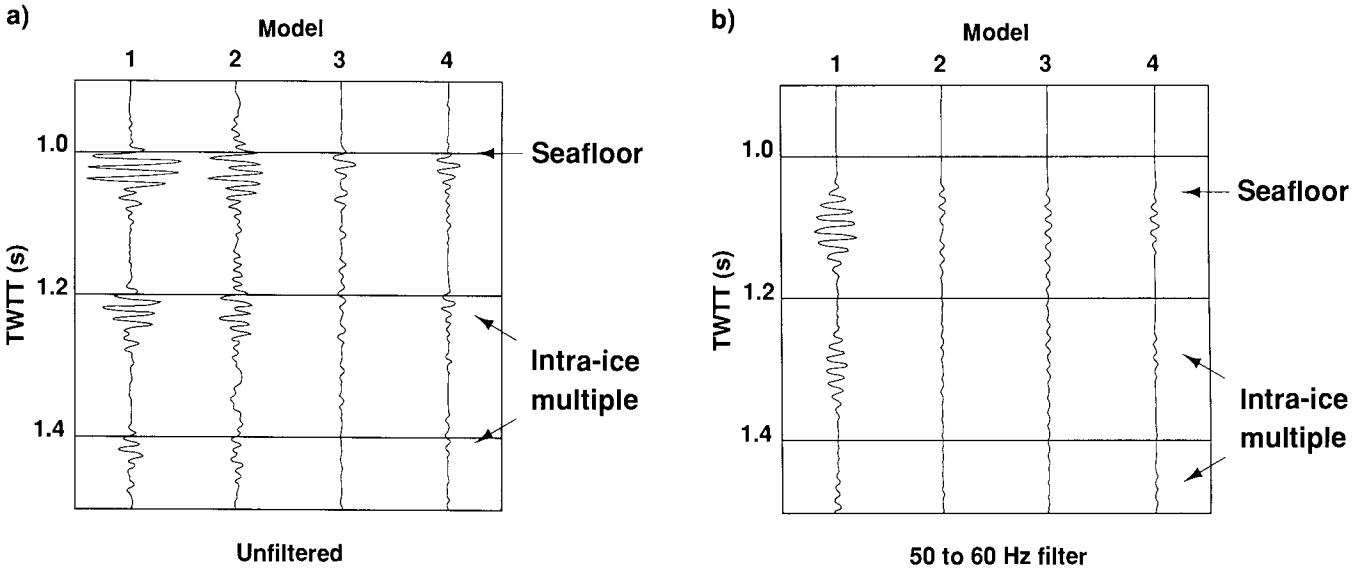

FIG. 7. (a) Unfiltered near-offset traces from the synthetic seismograms in Figure 6. (b) A 50 to 60 Hz band pass of the same traces. Only model 1 exhibits the amplification and frequency modulation observed in the data.

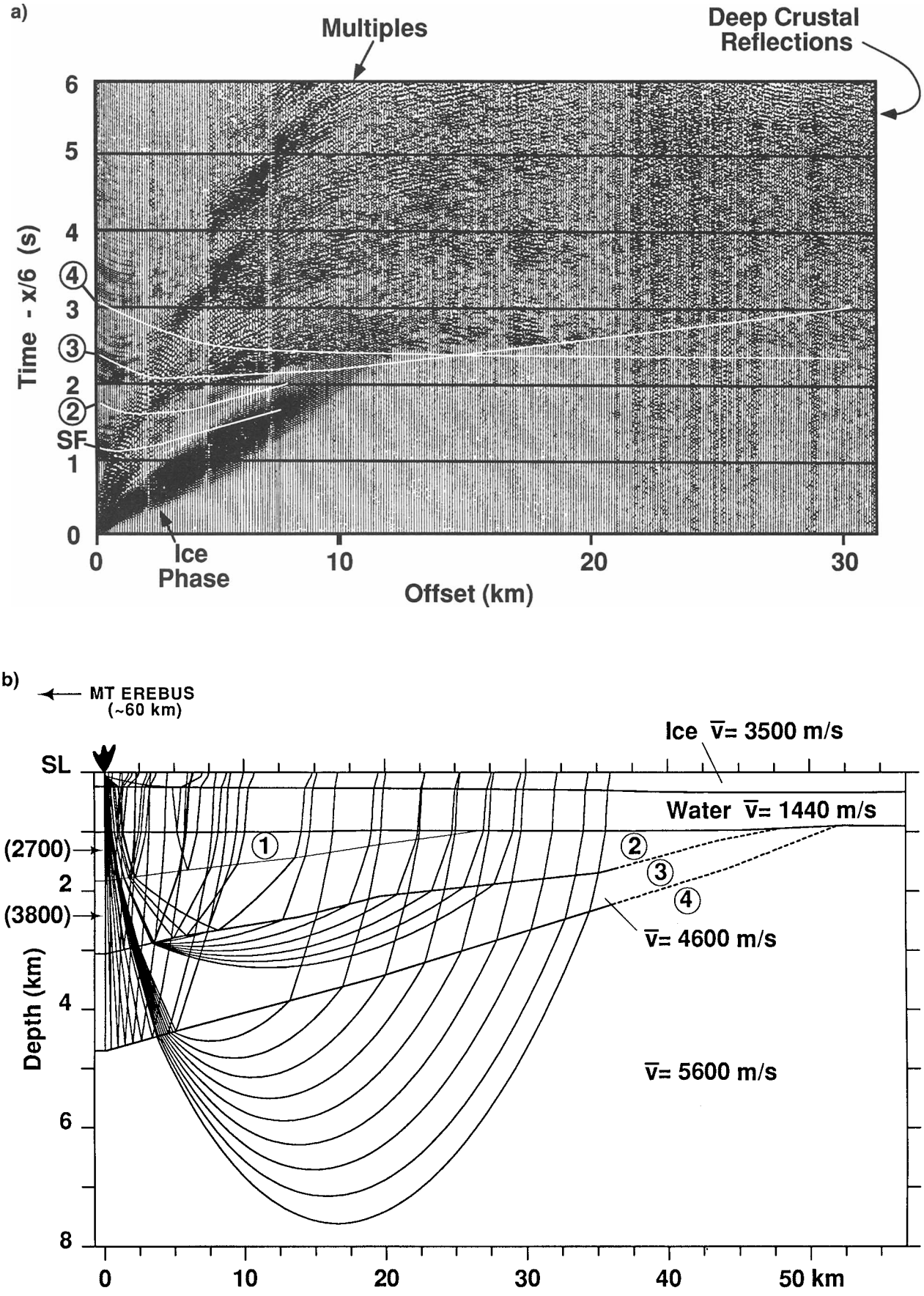

FIG. 9. (a) A filtered, laterally balanced, and trace-normalized display of the walk-away refraction profile with the calculated traveltimes overlain (white). (b) The ray diagram and compressional-wave velocity model used to produce the traveltime curves above. This common shot model is an approximation of the actual geometry. Velocities in (2700) are based on semblance.

Next a "pseudo" spiking deconvolution was applied to the data using a gap of two samples (4 ms). Using a traditional spiking deconvolution of one sample gap (2 ms), introduces low frequency overprints on the autocorrelations indicating that the wavelet is not minimum phase. This nonminimum phase wavelet is probably due to the precursor in energy from the 17 m of prima-cord (approximately 2 ms traveltime) used to detonate the main charge. It was determined that a constant operator length for the entire profile provided the best results, indicating that these are source reverberations and not dependent on the ice thickness. Both gap and "pseudo" spiking deconvolutions were applied after stack to further attenuate intra-ice multiple energy.

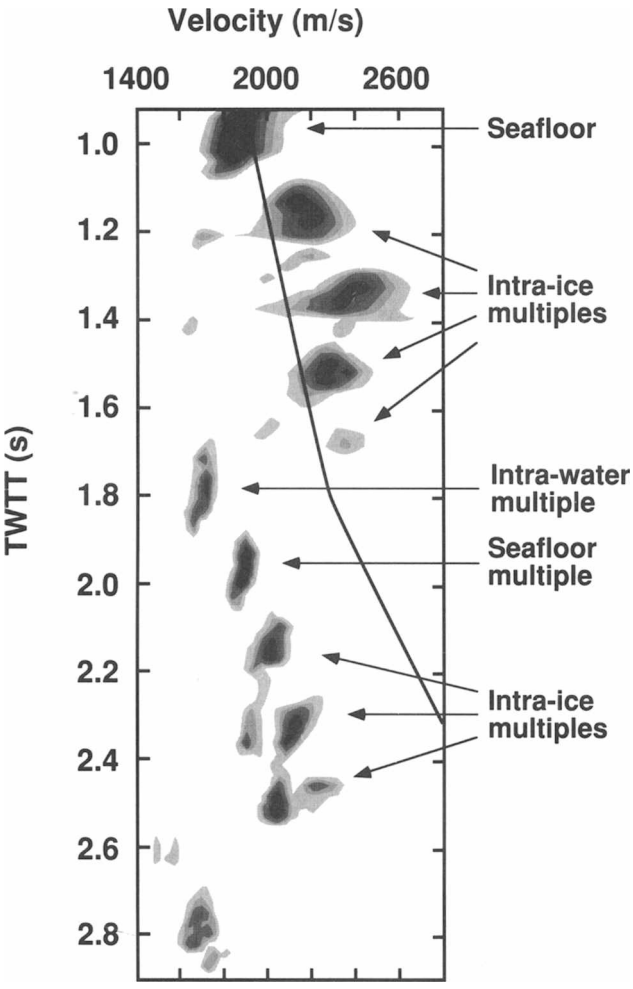

FIG. 10. A semblance plot of an unprocessed shot exemplifies the problems created by a thick, floating ice environment. Several multiple sets are clearly recognized. Overlain on the semblance plot is the one dimensional (1-D) velocity structure (heavy black line) obtained from the refraction profile. Note the substantial overlap of multiple velocities with our expected primary velocities within the first second below the seafloor.

Velocity filtering

Once the intra-ice multiples were significantly attenuated, processing focused on the long period seafloor and intra-water multiples. Several different approaches were taken but only one proved effective: an inverse velocity stacking method (Thorson, 1984; Hampson, 1986). Thorson (1984) devised the method of inverse velocity stacking to model hyperbolic events on seismic data. Hampson (1986) elaborated on this scheme applying it to long period multiple attenuation. To reduce computation time, Hampson's algorithm requires the data to have a normal moveout applied so events can be approximated with parabolas. This method models input data as a linear combination of parabolic events with constant amplitude. A series of weighting coefficients is derived such that the model fits the data in a least squares sense. Each parabolic event is characterized by an intercept time and residual moveout. By zeroing coefficients of unwanted energy after the transformation and then transforming back one can eliminate these events.

This technique was applied to shot gathers with normal moveout velocities determined from the refraction profile (Figure 9) and based on near-surface sediment velocities measure in the Ross Sea (Cooper et al., 1987). This method removed significant seafloor and intra-water multiple energy in addition to intra-ice multiple energy remaining after deconvolution (Figure 12).

Stacking

The final steps before frequency filtering included weighted stacking and poststack deconvolution as mentioned above. The velocity analysis was aided by the refraction profile (Figure 9). However, since the first 1.5 s below the seafloor show velocities lower than ice, no information on these layers is afforded by the refraction profile. For this portion of the section, both semblance and work done in the Ross Sea (Cooper et al., 1987) helped determine appropriate velocities. The final stack indicates that we have imaged several seconds of sediments overlying acoustic basement (Figure 13a). Below approximately 2.3 s on the northwest end and 2.0 s on the southeast end of the profile the quality of the stack deteriorates. This incoherent energy is left-over intra-ice multiple energy; this energy stacks with a velocity and periodicity consistent with intra-ice multiples from the first multiple set below the seafloor.

Frequency filtering

Frequency filtering provided a simple method to attenuate the multiples in the later part ($\geq$4 s) of the section. The intra-ice multiples have a low end frequency cutoff of around 25 Hz in the upper few seconds of the record (approximately 0 to 4 s) and are largely band limited to frequencies of greater than 40 Hz below this (Figure 3). These observations were used to construct the high end cutoff for the frequency filter. For the deeper portion of the reflection section ($\geq$4 s) a high cutoff of 40 Hz is sufficient to remove the intra-ice multiples. However, to retain resolution in the near seafloor section, a high end cutoff of 65 Hz is applied. This does not signifi-

cantly reduce the intra-ice multiples in the upper portion of the section and requires additional processing. For the low end cutoff, a frequency of 25 Hz is used just below the seafloor to reduce surface wave energy and 10 Hz in the lower portion of the section since no coherent events are evident below 10 Hz.

INTERPRETATION

We interpret the upper portion of the reflection profile as a wedge of sedimentary layers dipping toward Ross Island. Within this sedimentary wedge, stratigraphic relationships are chaotic. The lack of clear stratigraphic relations within the sedimentary wedge is likely due to the profile's resolution, 50 m CDP spacing. Stern et al. (1991) imaged a well stratified, near the seafloor, sedimentary section at the northern end of our profile with 17.5 m CDP spacing. Within the sedimentary wedge, the chaotic regions are separated by several continuous reflections (Figure 13a). These reflections appear to be truncated at or just below the seafloor suggesting an unconformable contact. It is possible that this unconformity is the Ross Sea Unconformity (Karl et al., 1987), observed in many profiles in the Ross Sea, that is attributed to the grounding of an advancing ice sheet at $\leq$10 Ma. Below this sedimentary wedge is a diffractive horizon which we interpret as the basement. There is an apparent onlapping relationship between the overlying sediments and the basement. Two normal faults are interpreted to displace the basement and the lowermost portion of the sedimentary sequence at 19 and 38 km along the profile.

Beneath the diffractive basement arrival several reflections of short lateral extent are observed (Figure 13b). These reflections have dips and arrival times that preclude them from being multiples. The most prominent of these is a 7.2 s arrival at the southeast end of the line (see Figure 3 and Figure 13b). Similar strong reflections at approximately 7 to 8 s have been observed in McMurdo Sound (McGinnis et al., 1985) and in the Ross Sea (Cooper et al., 1987; Trehu et al., 1989) and are interpreted as possibly Moho. Assuming the 7.2 s reflection is Moho, the crust beneath the profile is estimated to be 21-km thick based on an average crustal velocity of 6.5 km/s.

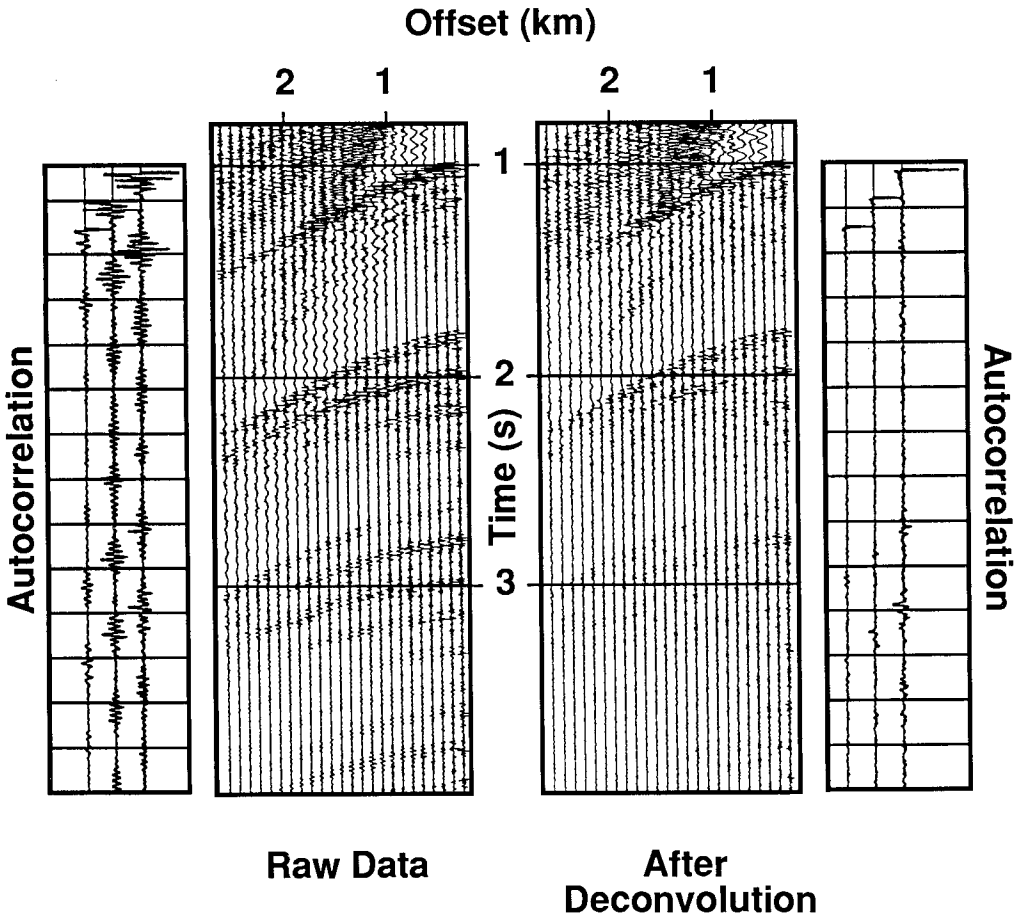

FIG. 11. An unfiltered shot gather before and after gap and "pseudo" spiking deconvolution with their respective autocorrelations of the first three traces.

CONCLUSIONS

The faulted basin structure underlain by a thin crust observed in these data is suggestive of extended crust. Based on these observations and the aforementioned geophysical studies, it is apparent that the extensional features observed in the Ross Sea region of the Ross Embayment extend beneath the Ross Ice Shelf. The implications of these observations are discussed in further detail in ten Brink et al. (in preparation).

Several suggestions for future work in similar environments, based on our experience with these data, are: (1) the near-surface firn layer is instrumental in shaping the seismic wavefield. For future experiments it is necessary to determine this near-surface velocity structure to effectively predict the multiple characteristics, (2) one of the main problems of working on the ice is the lack of energy penetration. A large portion of the source energy is trapped in the ice-water column. For this reason, expending the money, effort, and time to collect high-fold data and/or using larger shots, is an important consideration, and (3) in these data, the thickness of the ice-water column afforded simple muting of the ground roll. However, this is a very high energy, dispersive wave which in a thinner ice-water column setting would be very difficult to remove at our spatial sampling. Aside from resolution considerations, this indicates the need for having a small group interval.

Our success in attenuating multiples generated by the strong impedance across the ice-water interface is promising for future work on thick, floating ice. By demonstrating the use of standard processing techniques to achieve this goal, we have proven the feasibility for successful seismic imaging of the Ross Embayment beneath the Ross Ice Shelf and crustal imaging beneath the various ice shelves that rim the Antarctic continent.

ACKNOWLEDGMENTS

We thank our field party T. Hefford, K. Nicholas, I. Paintin, and P. Verhagen from New Zealand and R. Flanders, J. Kyne, and J. McGinnis from the U.S.A. for their monumental efforts in collecting these data, the Polar Ice Coring Office for drilling, and the employees of ITT Antarctic Services for their logistical support. In addition, we'd like to thank Jon Claerbout for the use of the Stanford Exploration Project CONVEX computer for the processing of these data. This work has been supported by NSF grant DPP-8813162 and by the Ross Dependency Research Committee grant under the United States-New Zealand cooperative science program.

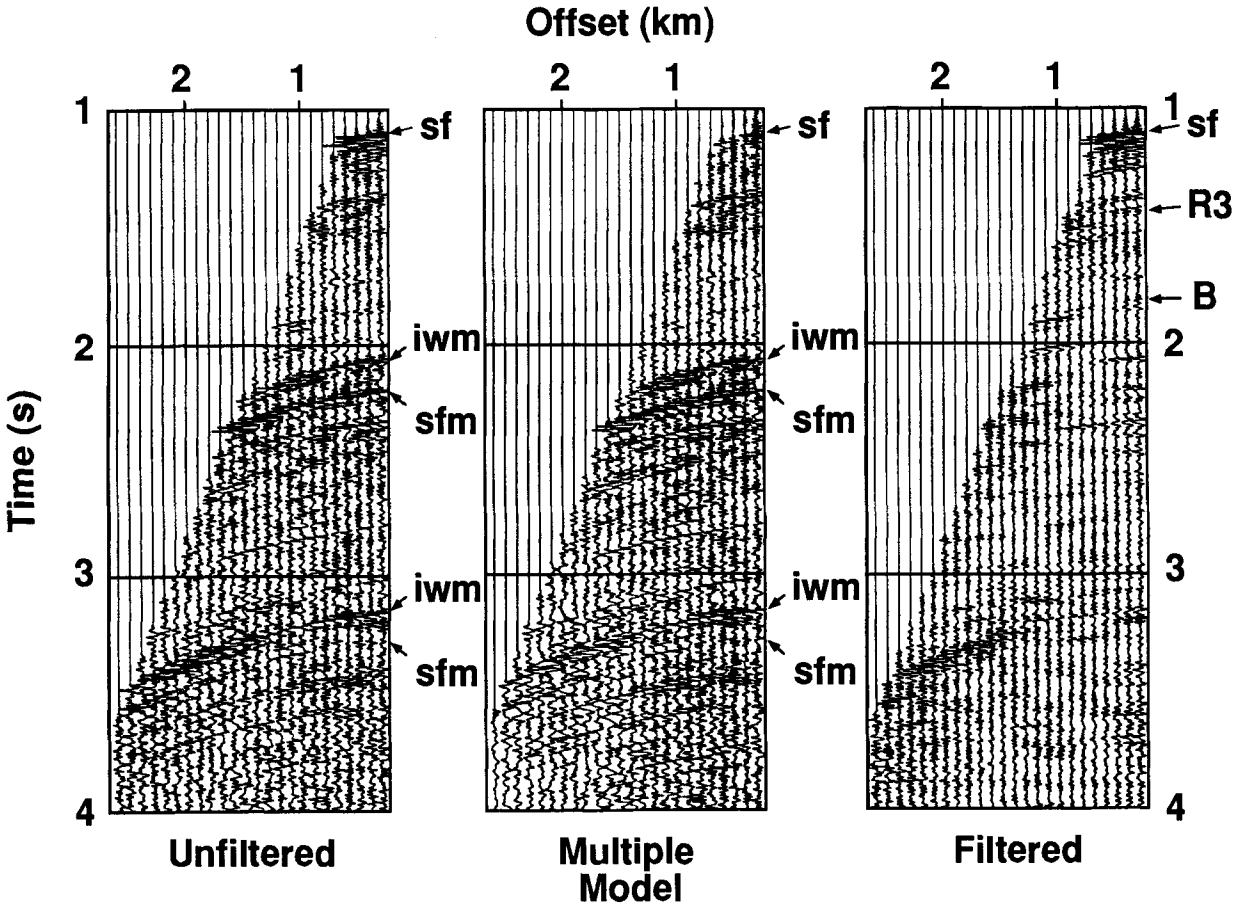

FIG. 12. The long period multiples modeled using an inverse velocity stacking filter (center) compared to unfiltered data (left) and the resultant filtered data (right). The identified phases are: sf, seafloor; iwm, intra-water multiple; sfm, seafloor multiple; R3 and B; interpreted sedimentary horizon and basement (see Figure 13).

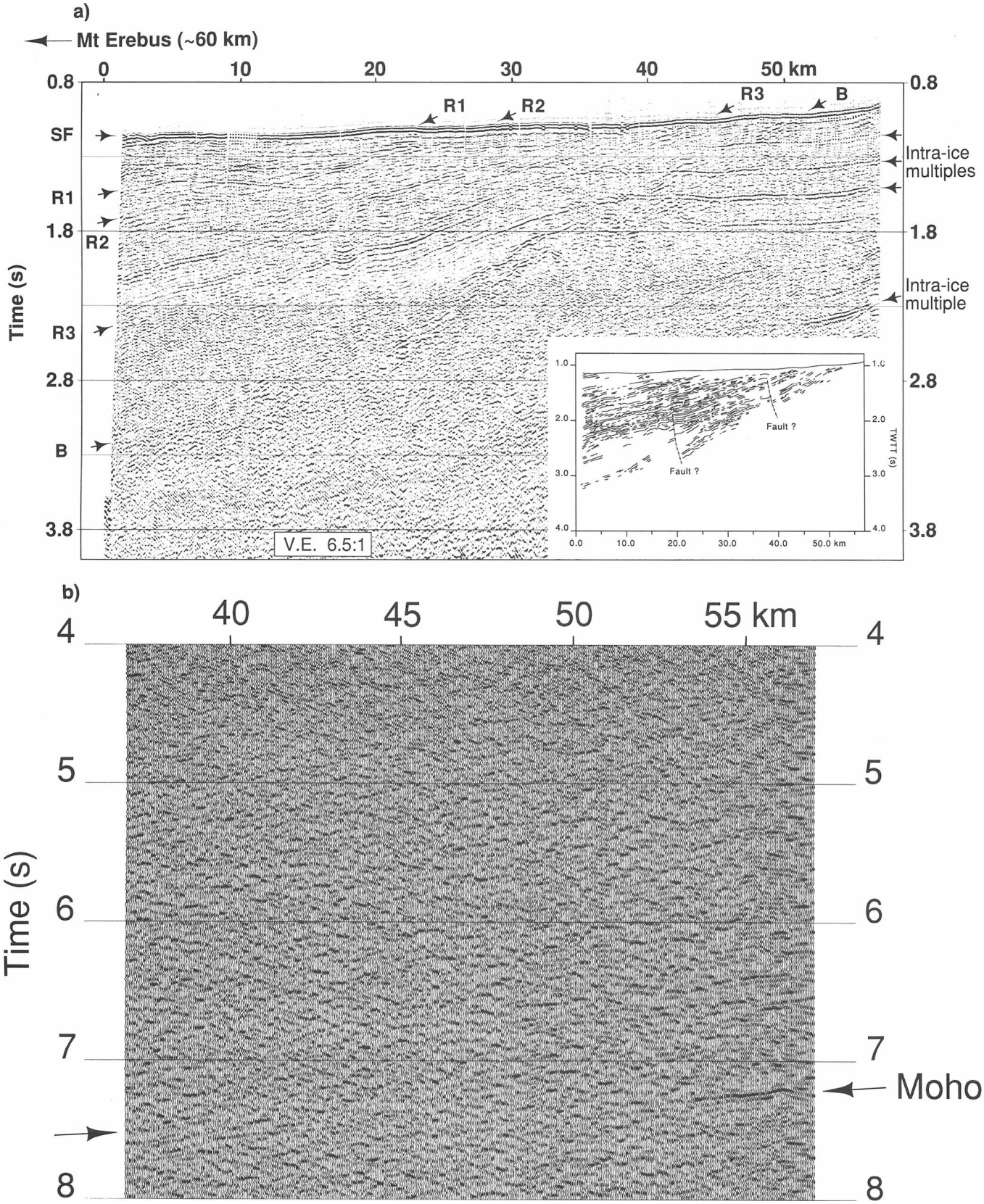

FIG. 13. (a) Final stacked section and line drawing interpretation. (b) A 4–8 s, 20-km-long section from the southeast end of the profile. The sections are six-fold, with 50 m CDP spacing. A time-variable filter and a 200 ms AGC were applied. The phases identified are: SF, seafloor; R1, R2, and R3, several of the more continuous reflectors; B, basement.

REFERENCES

Alam, A., and Austin, J., 1981, Suppression of multiples using slant stacks: Presented at the 51st Ann. Internat. Mtg., Soc. Expl. Geophys.

Anderson, D. L., and Benson, C. S., 1963, The densification and diagenesis of snow, *in* Kingery, W. D., Ed., Ice and snow: M.I.T. Press, 391–411.

Behrendt, J. C., and Cooper, A., 1991, Evidence of rapid Cenozoic uplift of the shoulder escarpment of the Cenozoic West Antarctic rift system and a speculation on possible climate forcing: Geology, **19**, 315–319.

Bentley, C. R., 1983, Crustal structure of Antarctica from geophysical evidence—A review, *in* Oliver, R. L., James, P. R., and Jago, J. B., Eds., Antarctic earth science: Cambridge Univ. Press, 491–497.

——— 1984, The Ross Ice Shelf geophysical and glaciological survey (RIGGS): Introduction and summary of measurements performed, *in* Bentley C. R., and Hayes, D. E., Eds., The Ross Ice Shelf: Glaciology and geophysics: Am. Geophys. Union, Antarctic Res. Series 42, 1–20.

Bentley, C. R., and Jezek, K. C., 1981, RISS, RISP, and RIGGS: Post-IGY glaciological investigations of the Ross Ice Shelf in the U. S. program: New Zealand, **11**, 355–372.

Beresford-Smith, G., and Rango, R. N., 1988, Dispersive noise removal in t-x space: Application to Arctic data: Geophysics, **53**, 346–358.

Blackman, D. K., Von Herzen, R. P., and Lawver, L. A., 1987, Heat flow and tectonics in the western Ross Sea, Antarctica, *in* Cooper A. K., and Davey F. J., Eds., The Antarctic continental margin: Geology and geophysics of the western Ross Sea: Circum-Pacific Council for Energy and Mineral Resources, 179–190.

Cooper, A. K., and Davey, F. J., 1985, Episodic rifting of Phanerozoic rocks in the Victoria Land Basin, western Ross Sea, Antarctica: Science, **229**, 1085–1087.

Cooper, A. K., Davey, F. J., and Cochrane, G. R., 1987, Structure of extensionally rifted crust beneath the western Ross Sea and Iselin Bank, Antarctica, from sonobouy seismic data, *in* Cooper A. K., and Davey F. J., Eds., The Antarctic continental margin: Geology and geophysics of the western Ross Sea: Circum-Pacific Council for Energy and Mineral Resources, 93–118.

Crary, A. P., Robinson, E. S., Bennett, H. F., and Boyd, W. W., Jr., 1962, Glaciological studies of the Ross Ice Shelf, Antarctica 1957–1960: Am. Geograph. Soc., Internat. Geophys. Yr. Glaciological Rep. No. 6.

Davey, F. J., Hinz, K., and Schroeder, H., 1983 Sedimentary basins of the Ross Sea, Antarctica, *in* Oliver, R. L., James, P. R., and Jago J. B., Eds., Antarctic earth science: Cambridge Univ. Press, 533–538.

Fitzgerald, P. G., Sandiford, M., Barrett, P. J., and Gleadow, A. J. W., 1986, Asymmetric extension associated with uplift and subsidence in the Transantarctic Mountains and Ross Embayment: Earth Planet. Sci. Lett., **81**, 67–78.

Fuchs, K., and Müller, G., 1971, Computation of synthetic seismograms with the reflectivity method and comparison with observations: Geophys. J. Roy. Astr. Soc., **23**, 417–433.

Hampson, D., 1986, Inverse velocity stacking for multiple elimination: J. Can. Expl. Soc. Geophys., **22**, 44–55.

Jankowski, E. J., and Drewry, D. J., 1981, The structure of west Antarctica from geophysical studies: Nature, **291**, 17–21.

Johnson, J. B., 1982, On the application of Biot's theory to acoustic wave propagation in snow: Cold Regions Sci. and Tech., **6**, 49–60.

Jurdy, D. M., 1978, An alternative model for early Tertiary absolute plate motions: Geology, **6**, 469–472.

Kamp, P. J., and Fitzgerald, P. G., 1987, Geologic constraints on the Cenozoic Antarctica-Australia-Pacific relative plate motion circuit: Geology, **15**, 694–697.

Karl, H. A., Reimnitz, E., and Edwards, B. D., 1987, Extent and nature of Ross Sea Unconformity in the western Ross Sea, Antarctica, *in* Cooper A. K., and Davey F. J., Eds., The Antarctic continental margin: Geology and geophysics of the western Ross Sea: Circum-Pacific Council for Energy and Mineral Resources, 77–92.

Kim, Y., McGinnis, L. D., and Bowen, R. H., 1986, The Victoria Land Basin: Part of an extended crustal complex between East and West Antarctica, *in* Barazangi, M. and Brown, L., Eds., Reflection Seismology: The Continental Crust: Am. Geophys. Union, Geodyn. Ser. 14, 323–330.

Kohnen, H., and Bentley, C. R., 1973, Seismic refraction and reflection measurements at "Byrd" station, Antarctica: J. Glaciol., **12**, 101–111.

Kyle, P. R., and Cole, J. W., 1974, Structural control of volcanism in the McMurdo Volcanic Group: Bull. Volcanol, **38**, 16–25.

Lang, T. E., 1976, Measurements of acoustic properties of hard-pack snow: J. Glaciol., **17**, 269–276.

McGinnis, L. D., Bowen, R. H., Erickson, J. M., Allred, B. J., and Kreamer, J. L., 1985, East-West Antarctic boundary in McMurdo Sound: Tectonophysics, **114**, 341–356.

Mertz, R. W., Brooks, L. D., and Lansley, M., 1981, Deepwater vibrator operations: Beauford Sea, Alaska, 1979 winter season: Geophysics, **46**, 172–181.

Press, F., and Ewing, M., 1951, Propagation of elastic waves in a floating ice sheet: Trans. Am. Geophys. Union, **32**, 673–678.

Proubasta, D., 1985, Ice saw - An incisive solution to seismic noise: The Leading Edge, **4**, no. 4, 18–23.

Rendleman, C. A., and Levin, F. K., 1990, Seismic exploration on a floating ice sheet: Geophysics, **55**, 402–409.

Robertson, J. D., and Bentley, C. R., 1975, Investigation of polar snow using seismic velocity gradients: J. Glaciol., **14**, 39–48.

Robertson, J. D., Bentley, C. R., Clough, J. W., and Greischar, L. L., 1982, Sea-bottom topography and crustal structure below the Ross Ice Shelf, Antarctica, *in* Craddock, C., Ed., Antarctic geoscience: Symposium on Antarctic Geology and Geophysics: Univ. of Wisconsin Press, 1083–1090.

Robinson, E. S., 1968, Seismic wave propagation on a heterogeneous polar ice sheet: J. Geophys. Res., **73**, 739–753.

Robinson, E. S., and Splettstoesser, J. F., 1984, Structure of the Transantarctic Mountains determined from geophysical surveys, *in* Turner, M. D., and Splettstoesser, J. E., Eds., Geology of the central Transantarctic Mountains: Am. Geophys. Union, Antarctic Research Series Volume 36, 119–162.

Stern, T. A., Davey, F. J., and Delisle, G., 1991, Lithospheric flexure induced by the loading of Ross Archipelago, southern Victoria Land, Antarctica, *in* Thomson, M. R. A., Crame, J. A., and Thomson, J. W., Eds., Geological evolution of Antarctica: Cambridge Univ. Press, 323–328.

Stock, J., and Molnar, P., 1987, Revised history of early Tertiary plate motion in the southwest Pacific: Nature, **325**, 495–499.

Thiel, E., and Ostenso, N. A., 1961, Seismic studies on Antarctic ice shelves: Geophysics, **26**, 706–715.

Thorson, J. R., 1984, Velocity-stack and slant-stack inversion methods: Ph.D. thesis, Stanford Univ.

Trehu, A. M., Holt, T., Behrendt, J. C., and Fitsch, J. C., 1989, Crustal structure in the Ross Sea, Antarctica - Preliminary results from GANOVEX V: Eos Trans. Am. Geophys. Union, **70**, 1344.

Wiggins, J. W., 1988, Attenuation of complex water-bottom multiples by wave-equation-based prediction and subtraction: Geophysics, **53**, 1527–1539.